Composite Structures xxx (2012) xxx–xxx

Contents lists available at SciVerse ScienceDirect

Composite Structures

journal homepage: www.elsevier.com/locate/compstruct

Masonry arches strehgthened with composite unbonded tendons

Angelo D'Ambrisi [a], Luciano Feo [b], Francesco Focacci [c,*]

[a] Dipartimento di Costruzioni e Restauro, Università di Firenze, Piazza Brunelleschi 6, 50121 Firenze, Italy
[b] Dipartimento di Ingegneria Civile, Università di Salerno, Via Ponte Don Melillo, 84084 Fisciano (SA), Italy
[c] Università eCampus, Via Isimbardi 10, 22060 Novedrate (CO), Italy

ARTICLE INFO

Article history:
Available online xxxx

Keywords:
Masonry arch
Unbonded composite tendon
Collapse mechanism
Finite displacements

ABSTRACT

In this paper an analytical model to evaluate the structural behavior of masonry arches and vaults strengthened with composite unbonded tendons placed at the extrados is presented. The tendons are fixed at the imposts. The model is formulated under the assumption of finite displacements. The displaced equilibrium configurations are identified by the stationarity of the potential of the acting forces. It is shown that when the tendon is not pretensioned an increase of the arch collapse load can be achieved only if the axial stiffness of the tendon is sufficiently large. Instead if the tendon is pretensioned an increase of the load that induces the first displacement of the arch is always achieved. If the stiffness of the tendon is sufficiently large the collapse load will be greater than the load that produces the first displacement of the arch.

1. Introduction

The load carrying capacity of masonry arches and vaults (Fig. 1) can be increased following two different strengthening strategies.

The first one consists in modifying the collapse mechanism of the structure using strengthening materials externally bonded at the intrados or the extrados surfaces. The strengthening material at the intrados (extrados) surface avoids the formation of hinges at the extrados (intrados) surface [1–3]. The modification of the collapse mechanism, that is related to the modification of the hinges positions, produces a consequent increase of the collapse load (Fig. 1b). Externally bonded fiber reinforced polymers (FRP) and fiber reinforced cementitious matrix (FRCM) are commonly used as strengthening materials within this context. In this case the key issue is the bond between the strengthening material and the support. The definition of the bond-slip relation is essential in the structural modeling of historical masonry constructions strengthened with composite materials, particularly when their seismic capacity is evaluated through nonlinear analyses [4,5]. This topic has been extensively investigated in the case of the FRP materials in many papers (e.g. [6,7]) while in the case of FRCM strengthening materials only a few research works have been performed [8–14].

The second strengthening strategy consists in the increase of the collapse load of the structure obtained contrasting the evolution of the collapse mechanism with an unbonded tendon placed at the extrados. In this case the evolution of the mechanism causes a tendon elongation and consequently an increase of the tendon tensile force which in turn contrasts the mechanism itself (Fig. 1c).

Experimental investigations relative to this strengthening strategy are presented in [15,16]. In these studies steel tendons were adopted. A strengthening of this type can be alternatively attained using tendons made of composite materials that can slip without friction inside a sheath. Rebars and tendon made of composite materials, although widely used in the cases of reinforcing and prestressing of concrete structures [17–19], have not yet been tested for the case analyzed in the present study.

An analytical model relative to a semicircular arch made of no tension material strengthened with an unbonded elastic tendon placed at the extrados is presented. The tendon is fixed at the arch imposts and it is supposed to slip without friction upon the extrados surface.

2. Analytical model

The mechanical model is formulated according to the following assumptions:

- the arch is made of no tension material [20–23], having an infinite compressive strength and stiffness; consequently a collapse mechanism is achieved both in the unstrengthened and strengthened configurations; this assumption results consistent with the actual structural behavior of unstrengthened masonry arches [24];
- the imposts are fixed for the presence of chains or massive abutments;

* Corresponding author. Tel.: +39 031 7942500; fax: +39 031 792631.
E-mail address: francesco.focacci@uniecampus.it (F. Focacci).

0263-8223/$ - see front matter © 2012 Elsevier Ltd. All rights reserved.
http://dx.doi.org/10.1016/j.compstruct.2012.10.040

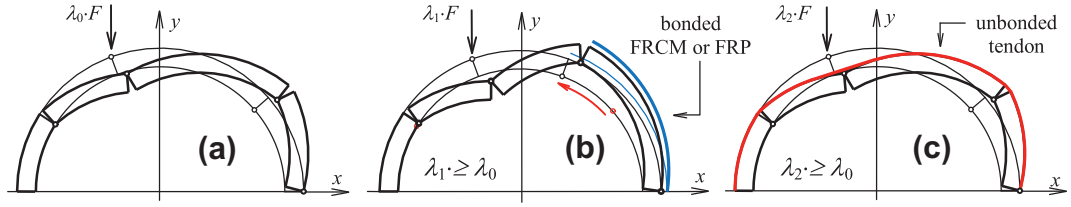

Fig. 1. Collapse of an (a) unstrengthened, (b) strengthened with externally bonded material and (c) strengthened with an unbonded tendon masonry arch.

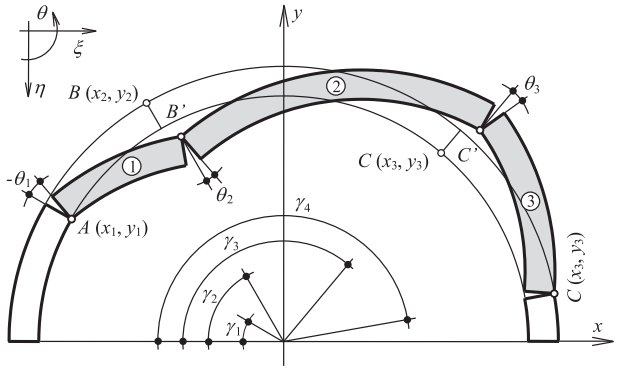

Fig. 2. Initial and generic configurations of the structure.

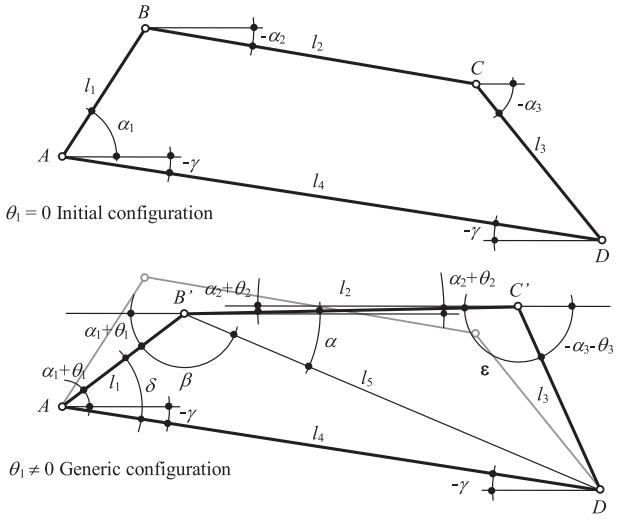

Fig. 3. Definition of geometric parameters.

- the tendon slips without friction at the extrados of the arch and it is fixed at the imposts;
- the tendon is made of a linear elastic composite material;
- the load configuration is constituted by the dead load (self weight and infill) and by an increasing vertical force;
- the unstrengthened arch does not collapse under the dead loads only;
- the collapse mechanism of the unstrengthened arch is characterized by four hinges placed as represented in Fig. 2;
- the hinges position minimizes the load producing the first displacement of the structure and does not change during its further displacements; this assumption is consistent with the fact that in a masonry arch the hinges can take place only at the mortar joints; this assumption could be removed in future studies on this topic.

The presented analytical model can be easily extended to a generic load configuration in which all the live loads are proportional to a load multiplier.

2.1. Geometry

A semicircular masonry arch (Fig. 2) with extrados and intrados radii R_e and R_i, respectively, a span $L_a = R_e + R_i$ and a thickness $s = R_e - R_i$ is considered. Four hinges having coordinates (x_j, y_j), $j = 1,\ldots,4$ in the system represented in Fig. 2 are considered.

The hinges positions are identified by the angles γ_j, $j = 1,\ldots,4$. The hinges position is such that if the hinge j is placed at the extrados, the hinges $j-1$ and $j+1$ are placed at the intrados and the quadrilateral having vertexes at the hinges is convex (Fig. 3).

Due to the presence of the hinges, the arch is divided into five rigid blocks. The three rigid blocks that can rotate are numbered so that the jth rigid block is delimited by the cross sections where the jth and $(j+1)$th hinges are located. In this configuration the arch is a system with one degree of freedom. The rotation of the first rigid block θ_1 is assumed as degree of freedom that identifies the generic configuration of the system. The rotation of the second and the third rigid blocks are θ_2 and θ_3. Counterclockwise rotations are considered positive. With reference to Figs. 2 and 3, the functions $\theta_2 = \theta_2(\theta_1)$ and $\theta_3 = \theta_3(\theta_1)$ are first determined, than the displacements of some points of interest are determined as a function of these rotations. l_1, l_2, l_3, l_4 are the sides of the quadrilateral having the vertex at the hinges. The lengths l_1, l_2, l_3, l_4 and the angles α_1, α_2, α_3, γ (Fig. 3) have to be preliminarily determined. If in the displaced configuration identified by $\theta_1 \neq 0$ the quadrilateral with the vertex at the hinges is still convex, it results

$$\theta_2(\theta_1) = \alpha_1 + \theta_1 + \alpha(\theta_1) + \beta(\theta_1) - \alpha_2 - \pi \tag{1}$$

where the angles $\alpha(\theta_1)$ and $\beta(\theta_1)$ are obtained as follows:

$$\alpha(\theta_1) = a\cos\frac{l_2^2 + l_5^2 - l_3^2}{2l_2l_5} \quad \beta(\theta_1) = a\cos\frac{l_1^2 + l_5^2 - l_4^2}{2l_1l_5} \tag{2}$$

where the length l_5 (Fig. 3) is

$$l_5(\theta_1) = \sqrt{l_1^2 + l_4^2 - 2l_1l_4\cos\delta} = \sqrt{l_1^2 + l_4^2 - 2l_1l_4\cos(\alpha_1 + \theta_1 - \gamma)} \tag{3}$$

The rotation of the second rigid block $\theta_2 = \theta_2(\theta_1)$ can be then expressed as

$$\theta_2(\theta_1) = \alpha_1 + a\cos\frac{l_1^2 + l_2^2 - l_3^2 + l_4^2 - 2l_1l_4a\cos(\alpha_1 + \theta_1 - \gamma)}{2l_2\sqrt{l_1^2 + l_4^2 - 2l_1l_4\cos(\alpha_1 + \theta_1 - \gamma)}} + a\cos\frac{2l_1^2 - 2l_1l_4\cos(\alpha_1 + \theta_1 - \gamma)}{2l_1\sqrt{l_1^2 + l_4^2 - 2l_1l_4\cos(\alpha_1 + \theta_1 - \gamma)}} - \alpha_2 - \pi \tag{4}$$

As concerns $\theta_3 = \theta_3(\theta_1)$, it results

$$\theta_3(\theta_1) = \varepsilon(\theta_1) + \alpha_2 + \theta_2(\theta_1) - \alpha_3 - \pi \tag{5}$$

where

Please cite this article in press as: D'Ambrisi A et al. Masonry arches strehgthened with composite unbonded tendons. Compos Struct (2012), http://dx.doi.org/10.1016/j.compstruct.2012.10.040

$$\varepsilon(\theta_1) = a\cos\frac{l_2^2+l_3^2-l_5^2}{2l_2l_3} = a\cos\frac{l_2^2+l_3^2-\left(l_1^2+l_4^2-2l_1l_4\cos(\alpha_1+\theta_1-\gamma)\right)}{2l_2l_3} \tag{6}$$

therefore

$$\theta_3(\theta_1) = a\cos\frac{l_2^2+l_3^2-l_1^2-l_4^2+2l_1l_4\cos(\alpha_1+\theta_1-\gamma)}{2l_2l_3}+\alpha_2 - \alpha_3+\theta_2(\theta_1)-\pi \tag{7}$$

where $\theta_2 = \theta_2(\theta_1)$ is expressed by Eq. (4).

The horizontal and vertical displacements ξ and η (Fig. 2) of the point (x,y) of the jth rigid block are

$$\begin{aligned}\xi_j(\theta_1) &= \xi_{hj}(\theta_1) - (x-x_j) + (x-x_j)\cos\theta_j - (y-y_j)\sin\theta_j\\ \eta_j(\theta_1) &= \eta_{hj}(\theta_1) + (y-y_j) - (y-y_j)\cos\theta_j - (x-x_j)\sin\theta_j\end{aligned} \tag{8}$$

where $\xi_{hj}(\theta_1)$ and $\eta_{hj}(\theta_1)$ are the horizontal and vertical displacements of the jth hinge

$$\begin{aligned}&\xi_{h1}(\theta_1) = \eta_{h1}(\theta_1) = 0\\ &\xi_{hj}(\theta_1) = \xi_{hj-1}(\theta_1) - (x_j-x_{j-1}) + (x_j-x_{j-1})\cos\theta_{j-1} - (y_j-y_{j-1})\sin\theta_{j-1}\\ &\eta_{hj}(\theta_1) = \eta_{hj-1}(\theta_1) + (y_j-y_{j-1}) - (y_j-y_{j-1})\cos\theta_{j-1} - (x_j-x_{j-1})\sin\theta_{j-1}\end{aligned} \tag{9}$$

2.2. Equilibrium configurations

The equilibrium configurations of the strengthened arch are identified by the stationarity condition of the potential $U = U(\theta_1)$ given by

$$U(\theta_1) = U_{SW}(\theta_1) + U_{DL}(\theta_1) + U_{LL}(\theta_1) + U_C(\theta_1) \tag{10}$$

where $U_{SW}(\theta_1)$ is the potential of the arch self weight, $U_{DL}(\theta_1)$ is the potential of the applied permanent loads, $U_{LL}(\theta_1)$ is the potential of the live loads and $U_C(\theta_1)$ is the elastic potential of the tendon. In the following, for the sake of simplicity, only the terms $U_{SW}(\theta_1)$, $U_C(\theta_1)$ and $U_{LL}(\theta_1)$ are considered. Moreover the live load is represented through a vertical force F applied at the extrados of the arch at the point identified by the angle γ_F (Fig. 4). More general cases, i.e. presence of infill or distributed live loads, can be easily solved in the same way.

2.2.1. Potential of the self weight

The vertical displacements η_{Gj} ($j = 1,2,3$) of the centers of mass of the three rigid blocks can be evaluated with Eq. (8)

$$\eta_{Gj}(\theta_1) = \eta_{hj}(\theta_1) + (y_{Gj}-y_j) - (y_{Gj}-y_j)\cos\theta_j - (x_{Gj}-x_j)\sin\theta_j \tag{11}$$

where the coordinates (x_{Gj},y_{Gj}) of the centers of mass of the rigid blocks in the initial configuration are

$$\begin{aligned}x_{Gj} &= -\frac{4}{3(\gamma_{j+1}-\gamma_j)}\frac{R_e^3-R_i^3}{R_e^2-R_i^2}\sin\frac{\gamma_{j+1}-\gamma_j}{2}\cos\frac{\gamma_j+\gamma_{j+1}}{2}\\ y_{Gj} &= \frac{4}{3(\gamma_{j+1}-\gamma_j)}\frac{R_e^3-R_i^3}{R_e^2-R_i^2}\sin\frac{\gamma_{j+1}-\gamma_j}{2}\sin\frac{\gamma_j+\gamma_{j+1}}{2}\end{aligned} \tag{12}$$

Then the potential of the self weight is

$$U_{SW}(\theta_1) = \sum_{j=1}^{3} W_j\eta_{Gj}(\theta_1) \tag{13}$$

where W_j is the weight of the jth rigid block.

2.2.2. Potential of the live load

The potential of the force F applied at the coordinates $x_F = -R_e\cos\gamma_F$, $y_F = R_e\sin\gamma_F$ is

$$U_{LL}(\theta_1) = F\eta_F(\theta_1) \tag{14}$$

where $\eta_F(\theta_1)$ is the vertical displacement o the point of application of the force. This displacement can be determined with Eq. (8).

2.2.3. Elastic potential of the tendon

A linear elastic tendon placed along the whole arch extrados and fixed at the imposts is considered (Fig. 4). The tendon has the elastic modulus E and the cross sectional area A. The tendon can be pretensioned by the force N_0 in the initial configuration $\theta_1 = 0$. The initial length of the tendon is $L_i = \pi\cdot R_e$. As the arch moves the tendon assumes the configuration that envelops the extrados the arch (Fig. 4) and therefore the length

$$L(\theta_1) = L_i + \Delta L = L_i + \Delta L_1 + \Delta L_3 - \Delta L_2 - \Delta L_4 \tag{15}$$

where ΔL_1 and ΔL_3 are the elongations at the intrados hinges 1 and 3, while ΔL_2 and ΔL_4 are the length decreases due to the detachment of the tendon at the extrados, close to the hinges 2 and 4 (Fig. 4). The elastic potential is

$$U_C(\theta_1) = -\left\{\frac{EA}{2\pi R_e}[\Delta L(\theta_1)]^2 + N_0\Delta L(\theta_1)\right\} \tag{16}$$

The elongations ΔL_1 and ΔL_3 are given by (Fig. 5)

$$\Delta L_1 = -2s\sin\frac{\theta_1}{2} \qquad \Delta L_3 = 2s\sin\frac{\theta_2-\theta_3}{2} \tag{17}$$

while the length decreases ΔL_2 and ΔL_4 are given by (Fig. 5)

$$\Delta L_2 = R_e\left(\theta_2-\theta_1-2\sin\frac{\theta_2-\theta_1}{2}\right) \qquad \Delta L_4 = R_e\left(-\theta_3-2\sin\frac{-\theta_3}{2}\right) \tag{18}$$

In Fig. 5 C_j is the center of the extrados arc of the jth rigid block ($j = 1,2,3$) in the generic configuration of the arch.

Eq. (18) are valid if the rotations are such that the tendon remains tangent to each rigid block, i.e. if the rotation θ_1 is not enough large to reach the configurations represented in Fig. 6. When the fourth hinge is at the impost the length decrease ΔL_4

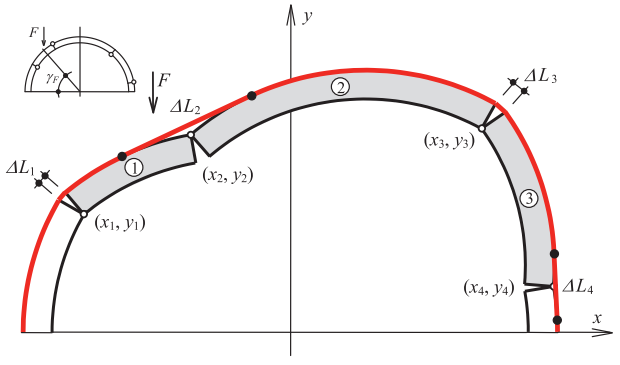

Fig. 4. Generic configuration of the arch.

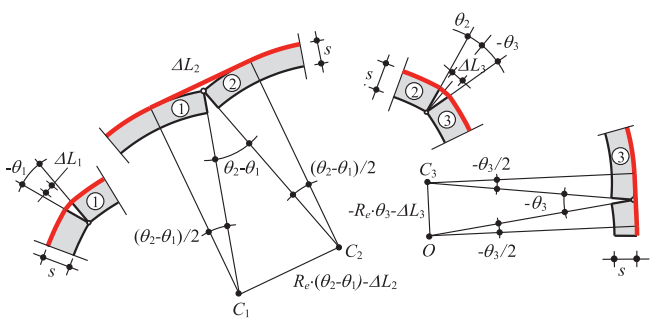

Fig. 5. Tendon deformation.

Please cite this article in press as: D'Ambrisi A et al. Masonry arches strehgthened with composite unbonded tendons. Compos Struct (2012), http://dx.doi.org/10.1016/j.compstruct.2012.10.040

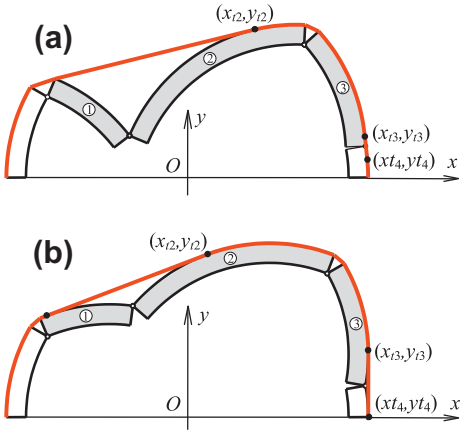

Fig. 6. Displaced configurations.

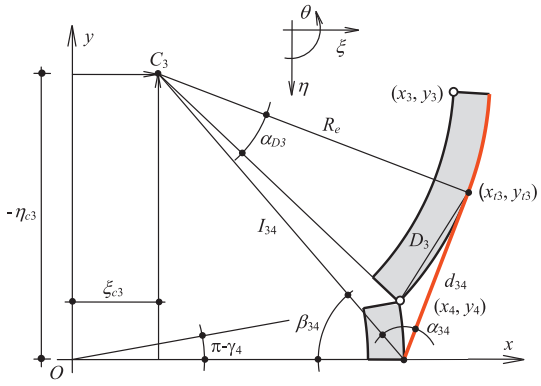

Fig. 7. Evaluation of ΔL_4 in the case $\gamma_4 < \pi$; $\xi_{c3} > 0$.

is instead null. The configuration in which the tendon is not tangent to the first rigid block (Fig. 6a) is reached for very large displacements, that are not of interest and therefore they are not considered. The configuration in which the tendon is not tangent to the fourth rigid block (Fig. 6b) is reached when the horizontal displacement $\xi_{C3}(\theta_1)$ of the center of the third rigid block is positive, that is when

$$\xi_{C3}(\theta_1) = \xi_{h3}(\theta_1) + x_3 - x_3\cos\theta_3 + y_3\sin\theta_3 \geqslant 0 \tag{19}$$

In this case, with reference to Fig. 7, the length decrease ΔL_4 is given by

$$\Delta L_4 = R_e(\pi - \gamma_4 + \alpha_{D3}) - d_{34} \tag{20}$$

where

$$\alpha_{D3} = 2a\sin\frac{D_3}{2R_e} = \frac{\sqrt{(x_4 - x_{t3})^2 + (y_4 - y_{t3})^2}}{2R_e} \tag{21}$$

while (x_{t3},y_{t3}) are the coordinates of the point of tangency between the tendon and the third rigid block

$$\begin{aligned} x_{t3} &= R_e + d_{34}\cos(\pi - \alpha_{34} - \beta_{34}) \quad y_{t3} \\ &= d_{34}\sin(\pi - \alpha_{34} - \beta_{34}) \end{aligned} \tag{22}$$

and (Fig. 7)

$$\alpha_{34} = a\sin\frac{R_e}{I_{34}} = a\sin\frac{R_e}{\sqrt{(R_e - \xi_{c3})^2 + \eta_{C3}^2}} \quad \beta_{34} = a\tan\frac{-\eta_{C3}}{R_e - \xi_{C3}} \tag{23}$$

$$d_{34} = \sqrt{I_{34}^2 - R_e^2} = \sqrt{(R_e - \xi_{C3})^2 + \eta_{C3}^2 - R_e^2} \tag{24}$$

in which η_{C3} is the vertical displacement of the center of the third rigid block

$$\eta_{C3}(\theta_1) = \eta_{h3}(\theta_1) - y_3 + y_3\cos\theta_3 + x_3\sin\theta_3 \tag{25}$$

Finally the length decrease ΔL_4 is given by

$$\Delta L_4 \begin{cases} R_e(\pi - \gamma_4 + D_{\alpha 3}) - d_{34} & \text{if } \gamma_4 < \pi \text{ and } \xi_{C3}(\theta_1) \geqslant 0 \\ R_e\left(-\vartheta_3 + 2\sin\dfrac{\theta_3}{2}\right) & \text{if } \gamma_4 < \pi \text{ and } \xi_{C3}(\theta_1) < 0 \\ 0 & \text{if } \gamma_4 = \pi \end{cases} \tag{26}$$

2.2.4. Equilibrium conditions

The total potential is then given by

$$\begin{aligned} U(\theta_1) = &\sum_{j=1}^{3} W_j\eta_{Gj}(\theta_1) + F\delta_F(\theta_1) \\ &- \left\{\frac{EA}{2\pi R_e}[\Delta L(\theta_1)]^2 + N_0\Delta L(\theta_1)\right\} \end{aligned} \tag{27}$$

The condition

$$\frac{dU}{d\theta_1} = 0 \tag{28}$$

allows to determine for each displaced configuration identified by θ_1 the corresponding equilibrium force

$$F = \frac{\dfrac{EA}{\pi R_e}\cdot\Delta L(\theta_1)\dfrac{d\Delta L(\theta_1)}{d\theta_1} + N_0\dfrac{d\Delta L(\theta_1)}{d\theta_1} - \displaystyle\sum_{j=1}^{3} W_j\frac{d\eta_{Gj}(\theta_1)}{d\theta_1}}{\dfrac{d\delta_F(\theta_1)}{d\theta_1}} \tag{29}$$

For $\theta_1 = 0$ Eq. (29) gives the force F_N^* that causes the first displacement of the arch (first displacement force). This force in the case of an unstrengthened arch is the collapse load. Eq. (29) evidences that this force is independent of the tendon stiffness since $\Delta L(0) = 0$. The first displacement force F_N^* and the corresponding hinges positions $\bar{\gamma} = \{\gamma_1, \gamma_2, \gamma_3, \gamma_4\}$ are determined minimizing Eq. (29) with respect the variables $\bar{\gamma} = \{\gamma_1, \gamma_2, \gamma_3, \gamma_4\}$ for $\vartheta_1 = 0$

$$F(\bar{\gamma}) = \frac{N_0\frac{d\Delta L}{d\theta_1}\Big|_0 - \displaystyle\sum_{j=1}^{3} W_j\frac{d\eta_{Gj}}{d\theta_1}\Big|_0}{\frac{d\delta_F}{d\theta_1}\Big|_0};$$

$$F_N^* = \min\{F(\bar{\gamma}), \bar{\gamma} = (\gamma_1\gamma_2, \gamma_3, \gamma_4) \in S \subset \Re^4\} \tag{30}$$

Eq. (30) shows that the hinges position is affected by the presence of the tendon only in the case $N_0 \neq 0$. The minimum of this function has to be searched in a suitable subset S of $\Re^4$ [1,24].

3. Analytical results

3.1. Strengthened arch with un-pretensioned tendon

Fig. 8 reports the $F - \theta_1$ curves obtained with Eq. (29) and the hinges positions obtained from Eq. (30) in the case $\gamma_F = \pi/4$ and $L_a/s = 16$ for an arch strengthened with an un-pretensioned tendon ($N_0 = 0$). The force is normalized with respect to the arch weight P.

Fig. 8 evidences that two different structural behaviors are possible depending on the tendon stiffness: large tendon stiffnesses lead to an increase of the collapse load with respect to the unstrengthened configuration (ascending branches of the $F - \theta_1$ curves), while small tendon stiffnesses do not affect the arch collapse load (descending branches of the $F - \theta_1$ curves). Therefore a limit stiffness $(EA)_{0-lim}$ can be defined such that tendon stiffnesses lower than $(EA)_{0-lim}$ do not produce increases of the collapse load, while tendon stiffnesses larger than $(EA)_{0-lim}$ lead to an increase of

Please cite this article in press as: D'Ambrisi A et al. Masonry arches strehgthened with composite unbonded tendons. Compos Struct (2012), http://dx.doi.org/10.1016/j.compstruct.2012.10.040

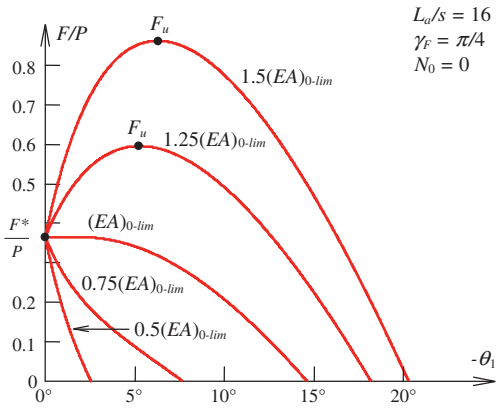

Fig. 8. $F - \vartheta_1$ curves in the case $N_0 = 0$.

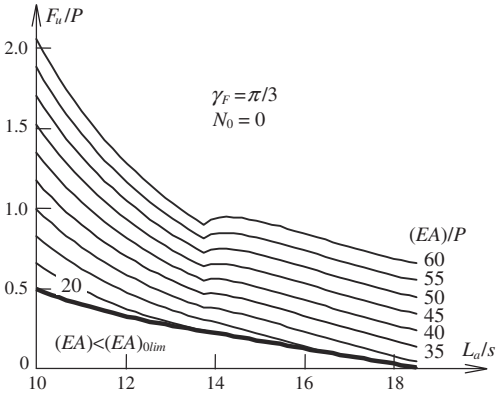

Fig. 11. F_u/P versus L_a/s in the case $\gamma_F = \pi/3$ and $N_0 = 0$.

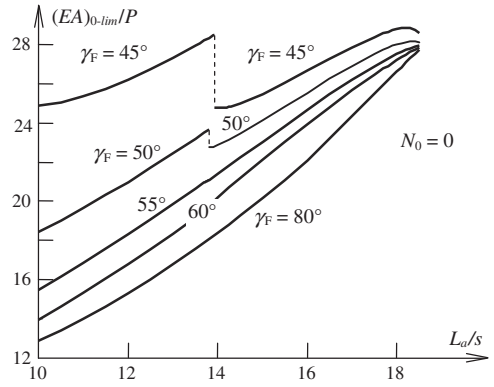

Fig. 9. $(EA)_{0-lim}/P$versus L_a/s curves for different force positions.

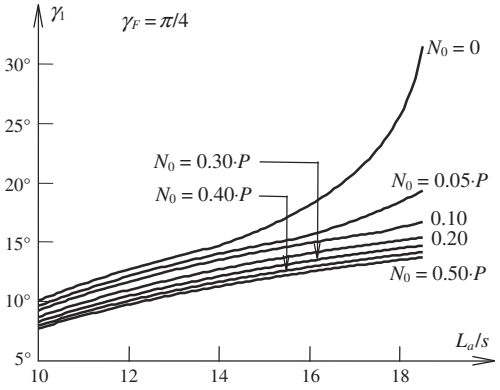

Fig. 12. Position γ_1 of the first hinge versus the ratio L_a/s.

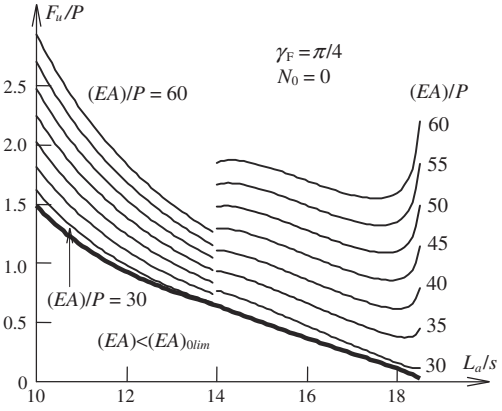

Fig. 10. F_u/P versus L_a/s in the case $\gamma_F = \pi/4$ and $N_0 = 0$.

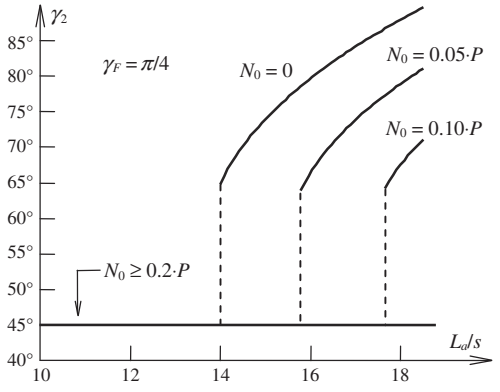

Fig. 13. Position γ_2 of the second hinge versus the ratio L_a/s.

the collapse load in the displaced configuration. The ratio between this stiffness and the arch weight P depends on the position γ_F of the force and on the ratio L_a/s as shown in Fig. 9.

Figs. 10 and 11 show the normalized collapse load F_u/P versus the ratio L_a/s curves for different tendon stiffenesses for the cases $\gamma_F = \pi/4$ and $\gamma_F = \pi/3$, respectively.

Figs. 12–14 show the dependence of the hinges positions on the ratio L_a/s and on the tendon pretension force N_0 for the case $\gamma_F = \pi/4$. The position of the fourth hinge does not depend on N_0 for the considered load condition. The discontinuity in Fig. 9 in the case $\gamma_F = \pi/4$ is due to the discontinuity of the hinges position as a function of the ratio L_a/s, as shown in Fig. 13.

3.2. Strengthened arch with pretensioned tendon

Fig. 15 reports the $F - \theta_1$ curves obtained with Eq. (29) and the hinges positions obtained from Eq. (30) in the case $\gamma_F = \pi/4$ and $L_a/s = 16$ for an arch strengthened with a pretensioned tendon with $N_0 = 0.2 \cdot P$.

The force is normalized with respect to the arch weight P. As it can be noticed the pretension increases the first displacement force from the value F^* to the value F^*_N. This force depends on N_0 and does not depend on the tendon stiffness as it is also evident from the Eq. (29). Also in this case a limit stiffness $(EA)_{lim}$ can be defined such that tendon stiffnesses lower than $(EA)_{lim}$ do not produce a

Please cite this article in press as: D'Ambrisi A et al. Masonry arches strehgthened with composite unbonded tendons. Compos Struct (2012), http://dx.doi.org/10.1016/j.compstruct.2012.10.040

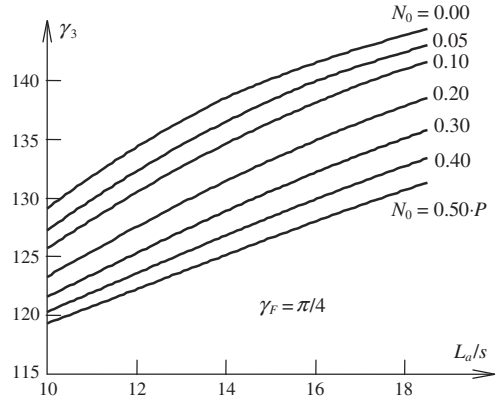

Fig. 14. Position γ_3 of the third hinge versus the ratio L_a/s.

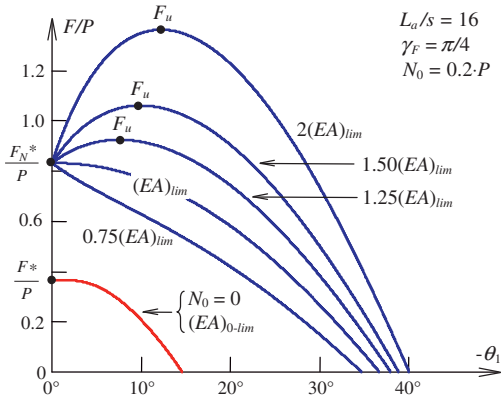

Fig. 15. $F - \vartheta_1$ curves in the case $N_0 = 0.2 \cdot P$.

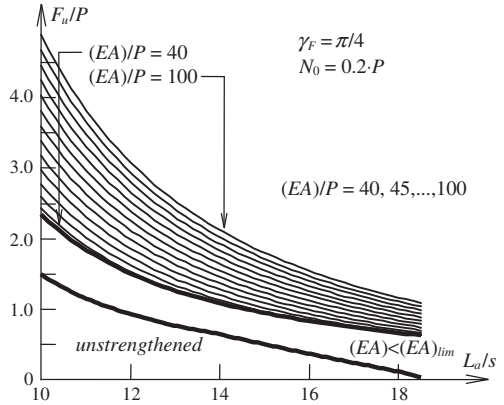

Fig. 16. F_u/P versus L_a/s in the case $\gamma_F = \pi/4$ and $N_0 = 0.2 \cdot P$.

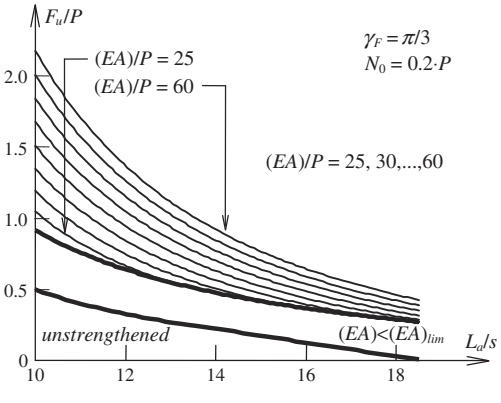

Fig. 17. F_u/P versus L_a/s in the case $\gamma_F = \pi/3$ and $N_0 = 0.2 \cdot P$.

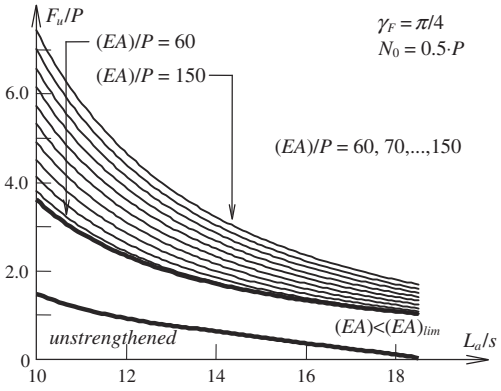

Fig. 18. F_u/P versus L_a/s in the case $\gamma_F = \pi/4$ and $N_0 = 0.5 \cdot P$.

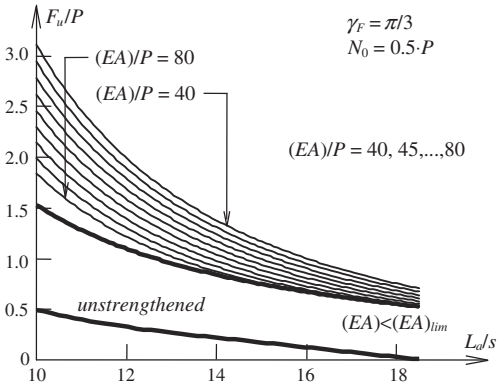

Fig. 19. F_u/P versus L_a/s in the case $\gamma_F = \pi/3$ and $N_0 = 0.5 \cdot P$.

collapse load larger than the first displacement load, while tendon stiffnesses larger than $(EA)_{lim}$ lead to a collapse F_u load larger than the first displacement load in the displaced configuration. The limit stiffness $(EA)_{lim}$ depends on the ratio N_0/P besides that on the ratio L_a/s. Figs. 16 and 17 show the normalized collapse load versus the ratio L_a/s for different tendon stiffnesses and for $N_0 = 0.2 \cdot P$, while Figs. 18 and 19 show the normalized collapse load versus the ratio L_a/s for different tendon stiffnesses and for $N_0 = 0.5 \cdot P$.

4. Conclusions

The proposed model allows to evaluate the effect of the strengthening of masonry arches and vaults with unbonded composite tendons placed at the extrados and fixed at the imposts. An increase of the load that produces the first displacement of the structure is obtained in the case of pretensioned tendons regardless of the tendon axial stiffness. A collapse load larger than the first displacement load is then obtained in the displaced configuration if the tendon is stiff enough. In the case of un-pretensioned tendons a collapse load larger than the first displacement load is obtained in the displaced configuration if the tendon is stiff

Please cite this article in press as: D'Ambrisi A et al. Masonry arches strehgthened with composite unbonded tendons. Compos Struct (2012), http://dx.doi.org/10.1016/j.compstruct.2012.10.040

enough. In particular for an arch with a span/thickness ratio of 16 strengthened with a tendon having a pretension force of 20% of the arch weight an increase of the first displacement load of about 300% is obtained.

Consistently with the last of the assumptions introduced in Section 2 the hinges position minimizes the load producing the first displacement of the structure and does not change during its further displacements. To remove this hypothesis and to include in the model the possibility that the arch collapse due to the masonry crushing or shear failure further studies are needed. The strengthening technique with extrados unbonded composite tendons fixed at the imposts confirms its effectiveness. It can be therefore considered in design applications of structural upgrading of masonry arches and vaults.

References

[1] Foraboschi P. Strengthening of masonry arches with fiber-reinforced polymer strips. J Compos Construct 2004;8(3):191–202.
[2] Rovero L, Focacci F, Stipo G. Structural behavior of arch models strengthened using FRP strips of different lengths. J Compos Construct, in press, http://dx.doi.org/10.1061/(ASCE)CC.1943-5614.0000325.
[3] Caporale A, Feo L, Luciano R. Limit analysis of FRP strengthened masonry arches via nonlinear and linear programming. Compos Part B: Eng 2012;43(2):439–46.
[4] Milani G, Milani E, Tralli A. Upper bound limit analysis model for FRP-reinforced masonry curved structures. Part II: Structural analyses. Comput Struct 2009;87(23–24):1534–58.
[5] D'Ambrisi A, Mariani V, Mezzi M. Seismic assessment of a historical masonry tower with nonlinear static and dynamic analyses tuned on ambient vibration tests. Eng Struct 2012;36:210–9.
[6] Carloni C, Subramaniam KV. Investigation of the interface fracture during debonding between FRP and masonry. Adv Struct Eng 2009;12(5):731–43.
[7] Carloni C, Subramaniam KV. FRP-masonry debonding: numerical and experimental study of the role of mortar joints. J Compos Construct 2012;16(5):581–9.
[8] D'Ambrisi A, Feo L, Focacci F. Experimental and analytical investigation on bond between Carbon-FRCM materials and masonry. Compos Part B: Eng, in press, http://dx.doi.org/10.1016/j.compositesb.2012.10.018.
[9] Carbone I, De Felice G. Debonding of C-FRCM composite on masonry support. In: Proc protection of historical buildings, PROHITECH 09, Rome, Italy; 2009.
[10] Faella C, Martinelli E, Paciello S, Perri F. Composite materials for masonry structures: the adhesion issue. In: Proc mechanics of masonry structures strengthened with composite materials, Venice, Italy; 2009.
[11] D'Ambrisi A, Feo L, Focacci F. Bond-slip relations for PBO-FRCM materials externally bonded to concrete. Composites: Part B 2012;43(8):2938–49.
[12] D'Ambrisi A, Feo L, Focacci F. Experimental analysis on bond between PBO-FRCM strengthening materials and concrete. Composites: Part B 2013;44(1):524–32.
[13] Carloni C, Sneed LH, D'Antino T. Interfacial bond characteristics of fiber reinforced concrete mortar for external strengthening of reinforced concrete members. In: Proc FraMCoS-8, Toledo, Spain; 2013.
[14] D'Ambrisi A, Focacci F. Flexural strengthening of RC beams with cement based composites. J Compos Construct 2011;15(5):707–20.
[15] Jurina L. L'arco armato nel consolidamento di archi e volte in muratura, Recupero e Conservazione 2000;33:54–61 [in Italian].
[16] Jurina L. Una tecnica di consolidamento attivo per archi e volte in muratura. In: Proc seismic performance of built heritage in small historic centers, Assisi, Italy; 1999. [in Italian].
[17] Saafi M, Toutanji H. Flexural capacity of prestressed concrete beams reinforced with aramid fiber reinforced polymer (AFRP) rectangular tendons. Construct Build Mater 1998;12(5):245–9.
[18] Toutanji H, Saafi M. Performance of concrete beams prestressed with aramid fiber-reinforced polymer tendons. Compos Struct 1999;44(1):63–70.
[19] Au FTK, Du JS. Deformability of concrete beams with unbonded FRP tendons. Eng Struct 2008;30(12):3764–70.
[20] Baratta A, Corbi O. An Approach to Masonry Structural Analysis by the No-Tension Assumption–Part I: Material Modeling, Theoretical Setup, and Closed Form Solutions. Appl. Mech. Rev. 2010;63(4).
[21] Baratta A, Corbi O. Analysis of the dynamics of rigid blocks using the theory of distributions. Advances in Engineering Software 2010;44(1):15–25.
[22] Foraboschi P. Coupling effect between masonry spandrels and piers. Materials and Structures 2009;42(3):279–300.
[23] Vanin A, Foraboschi P. In-Plane behaviour of preforated brick masonry walls. Materials and Structures 2012;45(7):1019–34.
[24] Heyman J. The Masonry Arch, Ellis Horwood Series in Engineering Science, UK, West Sussex, 115; 1982.

Please cite this article in press as: D'Ambrisi A et al. Masonry arches strehgthened with composite unbonded tendons. Compos Struct (2012), http://dx.doi.org/10.1016/j.compstruct.2012.10.040